Published online 17 June 2013 Nucleic Acids Research, 2013, Vol. 41, No. 16 7793–7803
doi:10.1093/nar/gkt483

TDP1 repairs nuclear and mitochondrial DNA damage induced by chain-terminating anticancer and antiviral nucleoside analogs

Shar-yin N. Huang[1], Junko Murai[1,2], Ilaria Dalla Rosa[1], Thomas S. Dexheimer[3], Alena Naumova[1], William H. Gmeiner[4] and Yves Pommier[1,*]

[1]Laboratory of Molecular Pharmacology, Center for Cancer Research, National Cancer Institute, National Institutes of Health, Bethesda, MD 20892, USA, [2]Department of Radiation Genetics, Kyoto University Graduate School of Medicine, Yoshida Konoe, Sakyo-ku, Kyoto 606-8501, Japan, [3]NIH Chemical Genomics Center, National Center for Advancing Translational Sciences, NIH, Rockville, MD 20850, USA and [4]Department of Cancer Biology, Wake Forest School of Medicine, Winston-Salem, NC 27157, USA

Received January 22, 2013; Accepted May 9, 2013

ABSTRACT

Chain-terminating nucleoside analogs (CTNAs) that cause stalling or premature termination of DNA replication forks are widely used as anticancer and antiviral drugs. However, it is not well understood how cells repair the DNA damage induced by these drugs. Here, we reveal the importance of tyrosyl–DNA phosphodiesterase 1 (TDP1) in the repair of nuclear and mitochondrial DNA damage induced by CTNAs. On investigating the effects of four CTNAs—acyclovir (ACV), cytarabine (Ara-C), zidovudine (AZT) and zalcitabine (ddC)—we show that TDP1 is capable of removing the covalently linked corresponding CTNAs from DNA 3′-ends. We also show that *Tdp1*$^{-/-}$ cells are hypersensitive and accumulate more DNA damage when treated with ACV and Ara-C, implicating TDP1 in repairing CTNA-induced DNA damage. As AZT and ddC are known to cause mitochondrial dysfunction, we examined whether TDP1 repairs the mitochondrial DNA damage they induced. We find that AZT and ddC treatment leads to greater depletion of mitochondrial DNA in *Tdp1*$^{-/-}$ cells. Thus, TDP1 seems to be critical for repairing nuclear and mitochondrial DNA damage caused by CTNAs.

INTRODUCTION

Chain-terminating nucleoside analogs (CTNAs) are widely used as antiviral and anticancer drugs (1,2). On incorporation into DNA, acyclovir (ACV), cytarabine (Ara-C), zidovudine (AZT) and zalcitabine (ddC) act as DNA chain terminators (Figure 1A). ACV, one of the earliest drugs in this class, is highly effective against herpesvirus infections (3); Ara-C is a widely used antileukemic drug (4); AZT and ddC are widely used for HIV infections (5). In the case of ACV, AZT and ddC, the high fidelity of human replicative DNA polymerases tends to limit their nuclear DNA incorporation, whereas the viral polymerases allow their incorporation into viral genomes. However, because of the large size of the human genome, exclusion of either drug is not absolute (6). Furthermore, antiviral-induced mitochondria toxicity has been reported and attributed to the less stringent selectivity of mitochondrial DNA polymerase (polγ) against antiviral CTNAs (7,8). By contrast, human DNA polymerases efficiently incorporate Ara-C during DNA synthesis, but its altered sugar structure prevents further DNA elongation (9–11) and ultimately kills cancer cells (12). Consequently, therapeutic CTNAs damage the nuclear or mitochondrial DNA of healthy cells (8,13). Some antivirals cause mitochondrial myopathy in patients undergoing long-term antiviral treatment (8,14). Yet, the pathways involved in removing the misincorporated CTNAs are not fully understood.

Discovered in yeast, tyrosyl–DNA phosphodiesterase 1 (TDP1) is a key enzyme for the repair of trapped topoisomerase I (Top1) cleavage complexes (15). TDP1-knockout mice and TDP1-deficient human cells are hypersensitive to Top1-targeting anticancer drugs, such as camptothecin (CPT) and its clinical derivatives topotecan and irinotecan (16–19). TDP1 also removes other 3′-blocking lesions in oxidative DNA damage repair, both in the nuclei and in mitochondria (20–23). A mutation in TDP1 causes the neurodegenerative disease spinocerebellar ataxia with axonal neuropathy (SCAN1) (20,24,25). These findings reflect the growing appreciation of TDP1's broad

*To whom correspondence should be addressed. Tel: +1 301 496 5944; Fax: +1 301 402 0752; Email: pommier@nih.gov

involvement in different types of DNA repair, which could account for its conservation in all eukaryotes (15).

In this study, we investigated the role of TDP1 in the excision repair of the four CTNAs.

MATERIALS AND METHODS

Preparation of radiolabeled oligonucleotide substrates

Except for 3′-Ara-C, all oligonucleotides were purchased from either Midland (Midland, TX, USA) or Integrated DNA Technologies (Coralville, IA, USA). All single-stranded DNA substrates share the common sequence of 5′-GATCTAAAAGACTT but bear different 3′-blocking lesions (26). The 3′-ACV was generated by incubating limiting amount of 3′-OH oligonucleotide with 100 μM of ACV-triphosphate from Sierra Bioresearch (Tucson, AZ, USA) in the presence of 3 U/μl of terminal deoxynucleotidyl transferase (Promega, Madison, WI, USA) at 37°C for 24 h. The 3′-Ara-C was synthesized using a universal support (Glen Research, Sterling, VA, USA) using cytidine arabinoside phosphoramidite (Chem Genes, Wilmington, MA, USA). The 3′-AZT was generated by first annealing 3′-OH with a longer complementary sequence with a 5′-overhang sequence of 5′-TTT**A**. The first nucleotide of the DNA duplex (opposite **A**) was then filled in by *Bsu* DNA polymerase (New England BioLabs, Cambridge, MA, USA) in the presence of 100 μM of AZT-triphosphate (Sierra Bioresearch, Tucson, AZ, USA). The product size corresponding to 3′-AZT was then gel purified and electroeluted. All oligonucleotides were labeled at the 5′-end with (γ-^{32}P) adenosine triphosphate (ATP) (PerkinElmer, Inc., Waltham, MA, USA) by T4 polynucleotide kinase from New England BioLabs (Cambridge, MA, USA). Double-stranded substrates were generated by annealing the 5′-radiolabeled single-stranded oligonucleotides with longer complementary strands. Thus, the substrates simulate a stalled replication fork with the 3′-blocking lesion at the recessed ends (overhang = 3 nt).

TDP1 reactions and gel analyses

Recombinant TDP1 was overexpressed and purified as previously described (27). QuikChange Site-Directed Mutagenesis Kit (Agilent Technologies, Santa Clara, CA, USA) was used to generate catalytic mutants of TDP1. In all, 1 nM labeled DNA substrates in a 10 μl reaction volume was incubated with recombinant human TDP1 at 25°C for 30 min. Reaction buffer contained 80 mM KCl, 2 mM ethylenediaminetetraacetic acid, 1 mM dithiothreitol, 40 μg/ml bovine serum albumin, 50 mM Tris–HCl, pH 7.5, and 0.01% Tween 20. Reactions were terminated by adding 1 volume of gel loading buffer [96% (v/v) formamide, 10 mM ethylenediaminetetraacetic acid, 1% (w/v) xylene cyanol and 1% (w/v) bromophenol blue]. Samples were analyzed by 16% denaturing polyacrylamide gel electrophoresis gels, which were dried and exposed on PhosphorImager screens. Imaging and quantification were done using a Typhoon 8600 and ImageQuant software (GE Healthcare, UK).

Kinetic measurements of TDP1

The oligonucleotide 3′-fluorescein was purchased from Integrated DNA Technologies (Coralville, IA, USA) with the shared sequence of 5′-GATCTAAAAGACTT. The oligonucleotide is linked to a 6-carboxyfluorescein (6-FAM) via a carbon linker on the 3′-end (donor), and the T in the sequence denotes a Tamra-dT (acceptor). From 100 to 500 nM of 3′-fluorescein substrate was mixed and incubated with 20 nM of TDP1 at 25°C in the reaction buffer aforementioned. The dead time of the reaction is <10 s, and the changes in fluorescein signal were monitored in real-time at 520 nm on a SpectraMax Germini XS microplate reader from Molecular Devices (Sunnyvale, CA, USA). The initial portions (180 s) of the traces were fitted to a linear equation to approximate the pre–steady-state reaction velocities. The processing of 100 and 200 nM 3′-fluorescein by 20 nM TDP1 was assumed to be at completion at the end of 1 h of data collection, and the end points of these two traces were used to convert the arbitrary units of fluorescence intensity into concentration of free fluorescein molecules processed by TDP1. Lineweaver–Burk plot was then generated with the pre–steady-state reaction velocities and the corresponding substrate concentrations.

Estimation of k_{cat}/K_M values of TDP1 for various substrates

All TDP1 reactions were carried out in the presence of the 1 nM substrate. Assuming the value of K_M is >1 nM (TDP1 has a K_M of 470 nM for 3′-fluorescein), it follows:

$$[S]_1 \approx [S]_2 \approx [S]_3 \approx \ldots \approx [S]_N << K_{MN}, v = \frac{k_{cat}}{K_M}[E]_t[S] = -\frac{\Delta[S]}{\Delta t}, \quad \frac{v_1}{v_2} = \frac{\frac{k_{cat1}}{k_{M1}}[E]_{t1}[S]_1}{\frac{k_{cat2}}{k_{M2}}[E]_{t2}[S]_2} \quad \exists v_1 = v_2, \ni \frac{k_{cat1}/K_{M1}}{k_{cat2}/K_{M2}} = \frac{[E]_{t2}}{[E]_{t1}} \tag{1}$$

where $[S]_N$ and K_{MN} are concentration and K_M values for each substrate, respectively. $[E]_t$ is the total concentration of enzyme.

Cell cultures

DT40 cells were cultured at 37°C with 5% CO_2 in Roswell Park Memorial Institute (RPMI-1640) medium supplemented with 1% chicken serum (Life Technologies, Carlsbad, CA, USA), 10^{-5} M β-mercaptoethanol, penicillin, streptomycin and 10% fetal bovine serum (FBS). Generation of *Tdp1*$^{-/-}$ DT40 cells were as previously described (23). Wild-type and *Tdp1*$^{-/-}$ murine embryonic fibroblasts (MEFs) were a kind gift from Dr Cornelius F. Boerkoel (Center for Molecular Medicine and

Therapeutics; University of British Columbia, Canada). MEF cells were cultured at 37°C with 5% CO_2 in Dulbecco's modified Eagle's medium (DMEM) containing 10% FBS (Life Technologies, Carlsbad, CA, USA).

Measurement of cellular sensitivity to DNA-damaging drugs

To measure the sensitivity of cells to ACV and Ara-C (Sigma-Aldrich, St. Louis, MO, USA), 200 DT40 cells were seeded in 384-well white plate (final volume 40 µl/well) from Perkin Elmer Life Sciences (Waltham, MA, USA) with the indicated drugs at 37°C. For MEF cells, 600 cells were seeded in 96-well white plate (final volume 100 µl/well) from Perkin Elmer Life Sciences (Waltham, MA, USA) and allowed to attach for 24 h at 37°C. Then the MEF cells were exposed to the indicated concentrations of drugs for 72 h with media change containing fresh drugs every 24 h. After 72 h, both DT40 and MEF cells were assayed in triplicates with the ATPlite 1-step kit (PerkinElmer, Waltham, MA, USA). Briefly, ATPlite solution was added to each well (20 µl for DT40 cells and 50 µl for MEF cells). After 5 min, luminescence intensity was measured by Envision 2104 Multilabel Reader from Perkin Elmer Life Sciences (Waltham, MA, USA). Signal intensities of untreated cells were set as 100%.

Clonogenic assays

To measure the survival rates of cells treated with ACV and Ara-C, 200 cells were seeded in triplicates in 4 ml of DMEM/F-12 clonogenic media containing the indicated drugs in six-well plates and incubated at 37°C. For clonogenic media, DMEM/F12 media (Life Technologies, Carlsbad, CA, USA) was supplemented with 15 g/l methylcellulose, 2 g/l $NaHCO_3$, 15% FBS, 10^{-5} M β-mercaptoethanol, 1.5% chicken serum and 2 mM L-glutamine (Life Technologies, Carlsbad, CA, USA). The number of colonies were manually counted after 14 days and averaged from triplicates; the viability of the untreated samples was set as 100%.

Cell cycle analyses

DT40 cells were continuously exposed to fixed concentrations of ACV or Ara-C at 37°C for 24 h. Harvested cells were fixed with 70% ethanol before re-suspension in phosphate-buffered saline containing 5 µg/ml propidium iodide. Samples were then subjected to analysis on an LSRFortessa cell analyzer from BD Biosciences (Franklin Lakes, NJ, USA).

Western blot analyses

Western blots were performed as described previously (23). Anti-γH2AX (ab22551, Abcam) and anti-β-actin (A5441, Sigma) primary antibodies were used at 1:3000 and 1:5000 dilutions, respectively.

Measurement of mitochondrial DNA copy number by quantitative real-time polymerase chain reaction

DT40 *Tdp1*$^{-/-}$ and wild-type cells were treated with indicated AZT or ddC (Sigma-Aldrich, St. Louis, MO, USA) concentrations, supplemented with 50 µM of uridine and incubated at 37°C for 24 h. The genomic DNA was extracted with Qiagen Dneasy Blood and Tissue Kit (Qiagen, Valencia, CA, USA) and used as templates in quantitative real-time polymerase chain reaction (PCR) with Power SYBR Green PCR Master Mix (Life Technologies, Carlsbad, CA, USA) in triplicates or quintuplets on an ABI 7900 thermocycler (Life Technologies, Carlsbad, CA, USA). Two sets of primers were used to selectively amplify the DT40 mitochondria genome or the s18-rRNA gene of the nuclear genome. The primers used to amplify the DT40 mitochondria genome are 5′-ccctcctcctttcatcctcatttc (sense) and 5′-ccttttttgttcaggcacgcttc (antisense). The primers used to amplify the s18-rRNA gene of the nuclear genome are 5′-tgactcaacacgggaaacctcac (sense) and 5′-ccagacaaatcgctccaccaac (antisense). The C_t value for mitochondria genome is referenced to the C_t value of the s18-rRNA for each sample. The ΔC_t for each sample is in turn referenced to that of the untreated control wild-type or *Tdp1*$^{-/-}$ cells ($\Delta\Delta C_t$), with the control of both cell types set at 1. The relative mtDNA copy number for each sample normalized to the untreated control is then calculated based on $\Delta\Delta C_t$ value of each sample.

RESULTS

TDP1 removes 3′-blocking CTNAs from DNA ends *in vitro*

We first investigated whether recombinant human TDP1 could remove the covalently linked CTNAs from the DNA 3′-end. To this end, we generated DNA substrates simulating a terminated DNA chain by attaching ACV, Ara-C or AZT to the 3′-end of a DNA oligonucleotide (Figure 1A). We examined TDP1 processing (Figure 1B) (28,29) of both CTNA-terminated and unmodified DNA (Figure 1A) (29). Incubation of TDP1 with each of the substrates containing 3′-blocking CTNAs generated a product that co-migrated with a marker that was one-nucleotide shorter and bore a 3′-phosphate group (Figure 1C), consistent with known TDP1 activity (26,29). We also verified that the processing of these substrates by TDP1 required its normal catalytic activity as the catalytically inactive mutants $TDP1^{H263A}$ and $TDP1^{H493R}$ (SCAN1 mutant) failed to process the substrates (Figure 1D).

Figure 1E shows quantification of TDP1 processing efficiency for each CTNA as a function of increasing TDP1 concentration. Under our experimental conditions, 3′-ACV was processed at a comparable rate as 3′-phosphoglycolate (3′-PG), a common oxidative DNA lesion and a known substrate for TDP1 (21). The 3′-ACV was a better substrate than its normal counterpart, deoxyguanosine (3′-dG), by >80-fold (Figure 1C and E). Both 3′-Ara-C and 3′-AZT were processed by TDP1 similarly to their respective normal counterparts, deoxycytidine (3′-dC), cytidine (3′-Ribo-C) and deoxythymidine (3′-dT) (Figure 1C) (Table 1). Processing efficiency of substrates bearing 3′-ddC by TDP1 was not tested. However, TDP1 processing of 3′-dC and 3′-Ribo-C displayed similar efficiency,

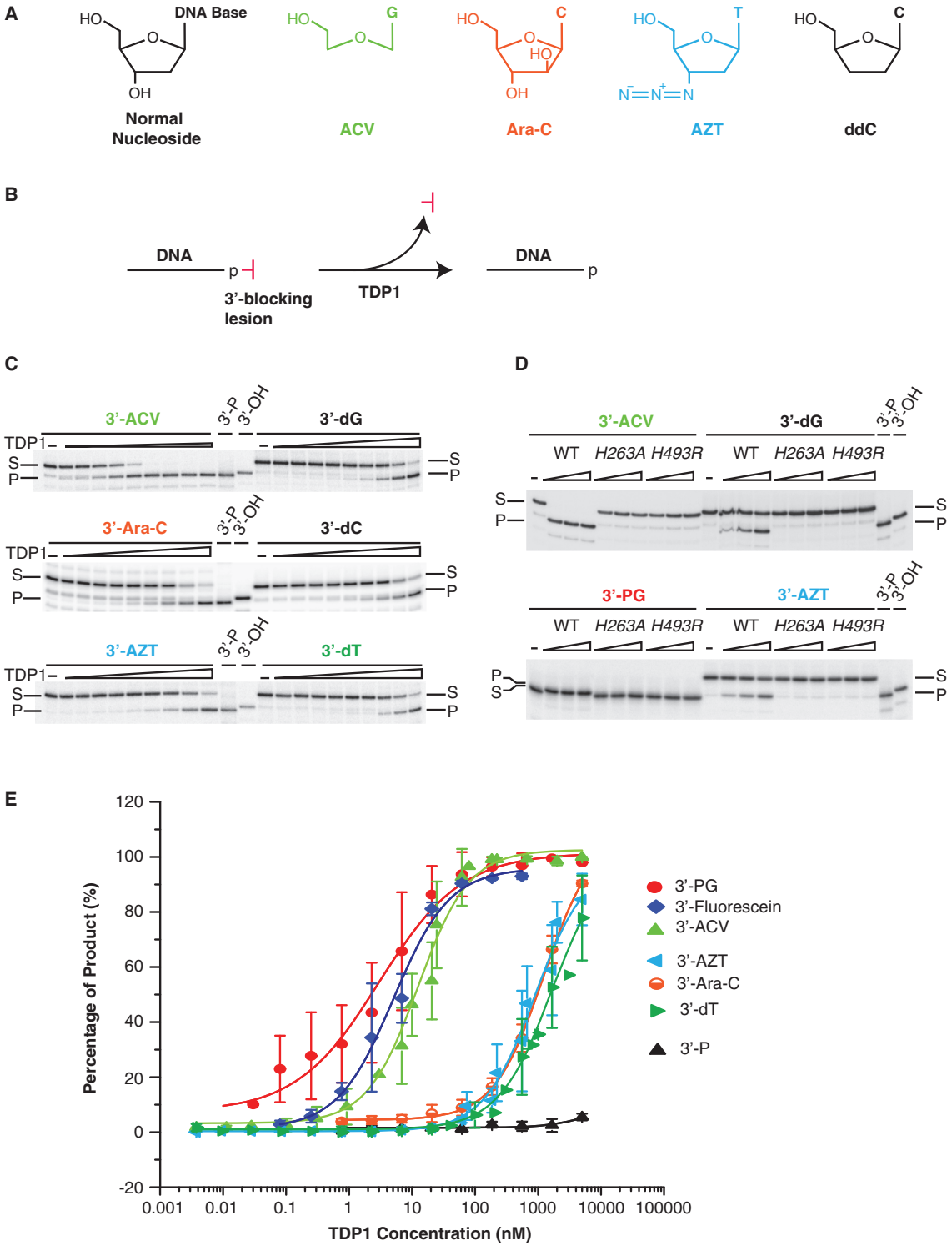

Figure 1. Processing efficiency of TDP1 for substrates containing various 3′-blocking lesions. (**A**) Structures of the DNA chain-terminating nucleoside analogs (CTNAs). (**B**) Schematic diagram of *in vitro* biochemical assays for TDP1 activity. (**C**) Representative gel images showing processing of the indicated substrates by increasing amount of TDP1. All substrates contained the same sequence, but bore different 3′-blocking lesions via a phosphodiester linkage, as indicated above each panel. The substrates (labeled S) were radiolabeled at the 5′-end with ^{32}P. Their products are labeled P. The 3′-ACV was incubated with serially diluted (1:3) TDP1 ranging from 0.08 to 555 nM. All the other substrates were incubated with serially diluted (1:3) TDP1 ranging from 0.8 nM to 5 μM. All reactions proceeded for 30 min at 25°C before being quenched and analyzed on 16% denaturing gels. Serving as markers, 3′-P and 3′-OH were oligonucleotides with a phosphate or a hydroxyl group on the 3′-end, respectively. (**D**) Processing efficiencies of various substrates by wild-type TDP1 and two catalytically deficient TDP1 mutants were tested in parallel: TDP1^{H263A} and TDP1^{H493R} (SCAN1 mutant). Each substrate was incubated at 25°C for 30 min with 111, 333 or 1000 nM of TDP1 proteins. The 3′-PG contained a 3′-phosphoglycolate lesion, a known substrate for TDP1. (**E**) The percentage of product yield is plotted against increasing TDP1 concentration in log-scale. Only selective 3′-blocking lesions are shown for the sake of clarity. At least three independent experiments (as in panel C) were quantified and averaged for each curve, and error bars represent SEM. Half maximal effective concentration (EC_{50}) for each substrate was determined by fitting the obtained curve to a sigmoidal model. The value of EC_{50} for each substrate is defined as $[E]_t$ in Equation (1).

Table 1. Specificity constants of TDP1 for various 3′-blocking lesions

The 3′-end blocking lesions	Specificity Constant at 25°C, k_{cat}/K_M (s^{-1} M^{-1})
3′-Y	9.1×10^7
3′-PG	2.4×10^5
3′-Fluorescein	1.4×10^5
3′-ACV	5.9×10^4
3′-AZT	8.3×10^2
3′-dG	7×10^2
3′-Ara-C	6×10^2
3′-dT	4×10^2
3′-Ribo-C	2.9×10^2
3′-dC	2.7×10^2
3′-dA	1×10^2
3′-P	9.7×10^{-5}

suggesting that the TDP1 processing of 3′-ddC should also be comparable. As controls, we included the reference substrate with a single tyrosine attached to 3′-DNA via a phosphodiester linkage (3′-Y) (Table 1). A second control substrate bearing a 3′-phosphate group (3′-P) was not processed at all even at the highest TDP1 concentration tested (Figure 1E) (Table 1) (26,29).

As stalling of the replication fork is the presumed consequence from treatment with CTNAs, we compared the ability of TDP1 to remove CTNAs from single-stranded versus double-stranded substrates. To simulate stalled replication forks, we used substrates with receding blocking ends (Figure 2, top right). We compared processing of 3′-ACV, 3′-Ara-C, 3′-AZT and 3′-Y in the two different contexts, and in each case, TDP1 prefers the single-stranded to the double-stranded substrates by 3–80-folds (Figure 2), consistent with previous reports for 3′-Y (30,31). Thus, our biochemical results demonstrate that

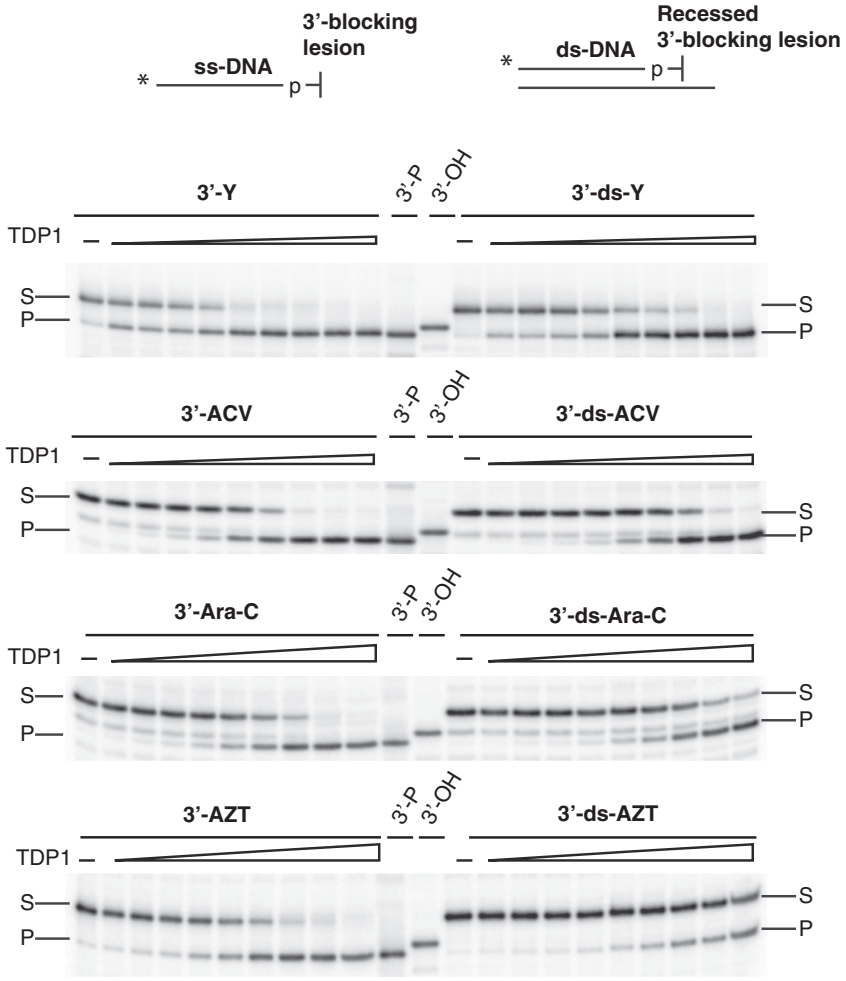

Figure 2. Processing efficiency of TDP1 for 3′-blocking lesions in single-stranded versus double-stranded DNA substrates. Representative gel images showing direct comparison of TDP1 processing 3′-blocking ends in single-stranded versus double-stranded substrates. All single-stranded substrates were the same as described in Figure 1C. For the double-stranded substrate, a longer complementary strand (+3 nt) was annealed to the strand containing 3′-blocking lesions, generating a recessed 3′-blocking lesion. The position of radiolabel with ^{32}P is noted with asterisk. The substrates and products are labeled S and P, respectively. Both 3′-Y and 3′ds-Y were incubated with serially diluted (1:2) TDP1 from 0.3 pM to 2.3 nM. Both 3′-ACV and 3′ds-ACV were incubated with serially diluted (1:3) TDP1 ranging from 0.8 nM to 5 μM. All the other substrates were incubated with serially diluted (1:3) TDP1 ranging from 2.3 nM to 15 μM. All reactions proceeded for 30 min at 25°C before being quenched and analyzed on 16% denaturing gels. Markers 3′-P and 3′-OH were the same as described in Figure 1C.

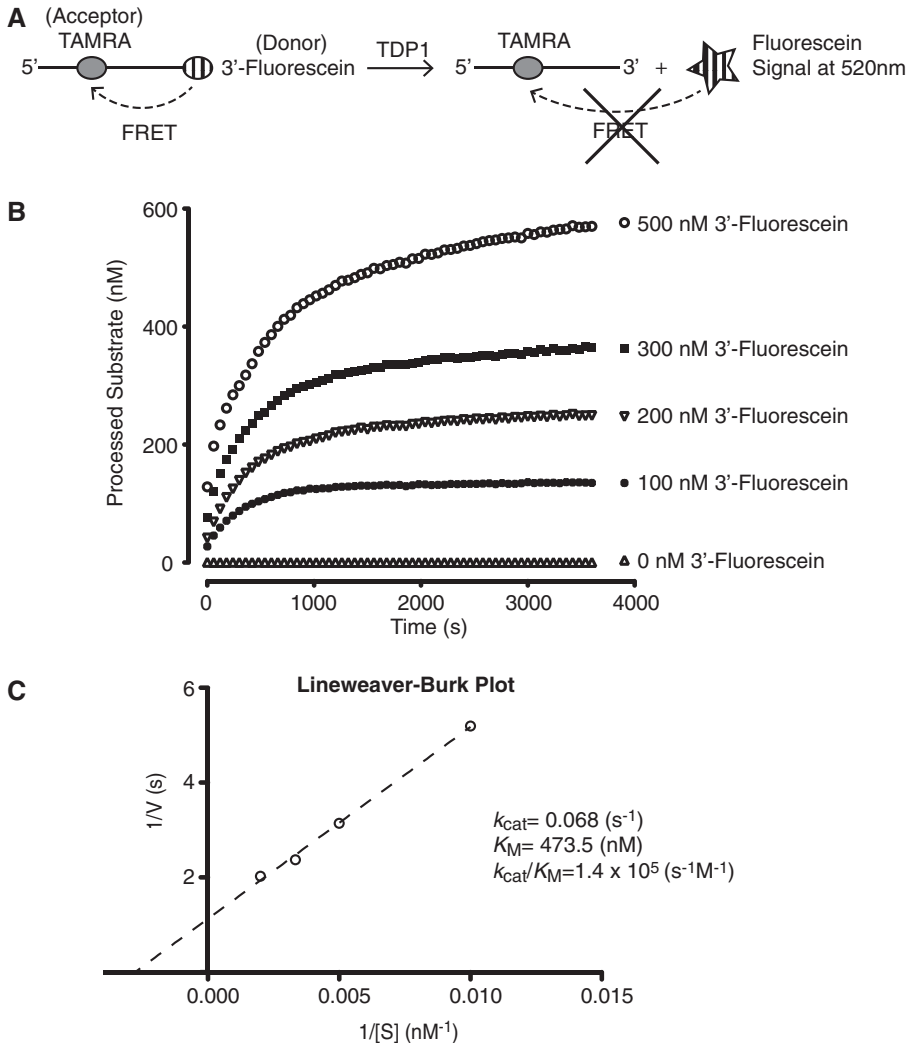

Figure 3. Real-time processing kinetics of TDP1 for substrates containing 3′-fluorescein. (**A**) Schematic diagram of the FRET-based substrate is shown. Fluorescein is attached to the 3′-phosphate group of the oligonucleotide via a short carbon linker. The oligonucleotide is internally labeled with a carboxytetramethylrhodamine (TAMRA), which acts as an acceptor for the fluorescein. Once TDP1 cleaves off the fluorescein group, FRET is abolished, and the free fluorescein gives rise to a signal. (**B**) The indicated concentrations of 3′-fluorescein were incubated with 20 nM TDP1 at 25°C, and the changes in fluorescein signal were monitored in real-time at 520 nm. The initial linear portions of the traces (0–180 s) were fit to a linear equation to generate pre–steady-state reaction velocities. (**C**) Lineweaver–Burk plot generated from the calculated reaction velocities from data in panel B is shown.

TDP1 removes 3′-blocking CTNAs from single-stranded or recessed DNA ends *in vitro*.

To quantitate the relative efficiency of TDP1 for the different CTNAs, we measured pre–steady-state kinetics for fluorescence resonance energy transfer (FRET)-based substrate (3′-fluorescein) (Figures 1E and 3A). Based on the specificity constant (k_{cat}/K_m) of TDP1 measured for 3′-fluorescein (Figure 3B and C), we estimated the specificity constants for all the other TDP1 substrates (Table 1). The specificity constant for each substrate is essentially inversely related to the amount of enzyme required to achieve the same processing rate under the same experimental conditions [Equation (1) in the 'Materials and Methods' section]. The calculated specificity constant of TDP1 for 3′-Y was $9 \times 10^7 s^{-1} M^{-1}$, in good agreement with previous reports (32,33). TDP1 specificity constants for 3′-ACV and 3′-PG were similar, whereas the 3′-blocking lesions formed by all the other CTNAs shared comparable specificity constants that were ~100-fold lower (Table 1). Note that the processing efficiency of TDP1 for 3′-CTNAs was close to values reported for phospholipase-D, another enzyme in the same superfamily as TDP1 (34), positioning these substrates in potentially physiologically relevant range for TDP1 *in vivo*.

Tdp1$^{-/-}$ cells are hypersensitive to CTNAs

Next, we investigated TDP1's role in repairing CTNA-induced DNA damage *in vivo*. Judging from ATP activity measurements, *Tdp1*$^{-/-}$ DT40 cells (23) consistently showed hypersensitivity to ACV and Ara-C (Figure 4A). In contrast, *Tdp1*$^{-/-}$ DT40 cells were not hypersensitive to gemcitabine (Figure 4A), a chemotherapeutic CTNA,

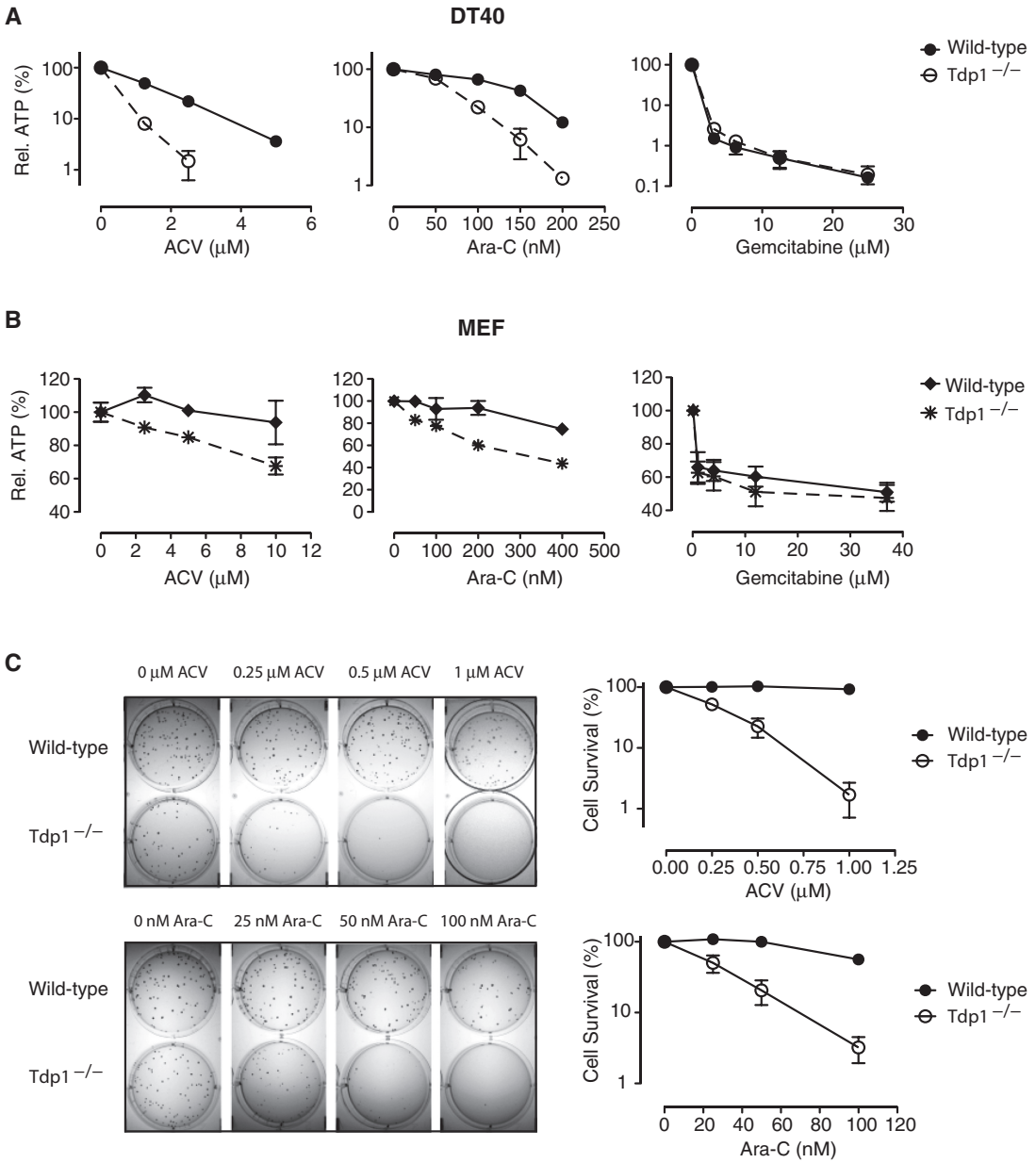

Figure 4. Hypersensitivity of *Tdp1*$^{-/-}$ cells derived from chicken DT40 and MEF cells to CTNAs. Relative ATP contents of wild-type and *Tdp1*$^{-/-}$ cells were compared for both (**A**) DT40 and (**B**) MEF cells. Cells were treated with the indicated drugs continuously for 72 h, at which time cells were assayed using ATP-lite. The signal for untreated cells was set as 100%. Error bars represent SD ($n = 3$). (**C**) Representative pictures and quantification of clonogenic assays for wild-type and *Tdp1*$^{-/-}$ DT40 cells are shown. The cells were treated with indicated drugs in triplicates for 14 days, at which time the number of colonies for each well was manually counted. The viability of the untreated cells was set as 100%. Error bars represent SEM ($n = 3$).

which we used as a negative control. Indeed, gemcitabine functions via a different biochemical mechanism in which it does not immediately terminate DNA chain elongation on incorporation but stops elongation after incorporation of additional nucleotides (35). The calculated half maximal inhibitory concentration (IC_{50}) values after 72 h are listed in Table 2.

The DT40 results were confirmed in *Tdp1*$^{-/-}$ MEF cells (16), which also showed hypersensitivity toward ACV and Ara-C, albeit to lesser extents than DT40 cells (Figure 4B). Similar to DT40 cells, *Tdp1*$^{-/-}$ MEF cells were not hypersensitive to gemcitabine (Figure 4B). As ACV and Ara-C did not reach IC_{50} in the less sensitive MEF cells in the concentration range tested, only IC_{50} values of DT40 cells were listed in Table 2. The difference in drug sensitivity between DT40 and MEF cells could be due to difference in transport, activation and/or incorporation of CTNAs.

To confirm that treatment with CTNAs compromised the viability of *Tdp1*$^{-/-}$ cells, we performed clonogenic assays. The results showed that *Tdp1*$^{-/-}$ DT40 cells were

clearly hypersensitive toward ACV and Ara-C in a dose-dependent fashion (Figure 4C). The consistent hypersensitivity of both *Tdp1*$^{-/-}$ DT40 and MEF cells in assays based on ATP content and clonogenic survival implicate TDP1 in the repair of ACV- and Ara-C-induced DNA damage.

Increased DNA damage induced by CTNAs in *Tdp1*$^{-/-}$ cells

To further characterize the differential response of wild-type and *Tdp1*$^{-/-}$ cells to CTNAs, we carried out cell cycle analyses. The cell cycle profiles of untreated wild-type and *Tdp1*$^{-/-}$ cells were essentially indistinguishable (Figure 5A), consistent with our previous finding that TDP1 deficiency has no detectable effect on DT40 cells in the absence of DNA damage (23). Treatment of wild-type cells with ACV or Ara-C for 24 h arrested cells in S-phase and induced a small sub-G_1 (cell death) population (Figure 5A), consistent with the drugs' mild but detectable adverse effect on the wild-type cells (Figure 4). In the case of the *Tdp1*$^{-/-}$ cells, the cell cycle profile alteration was more pronounced. The treated *Tdp1*$^{-/-}$ DT40 cells showed a marked increase in sub-G_1 population and a more pronounced S-phase arrest compared with wild-type cells (Figure 5A), consistent with the greater cytotoxic effect of CTNAs on *Tdp1*$^{-/-}$ cells (Figure 4).

Western blots of wild-type and *Tdp1*$^{-/-}$ DT40 cells treated with ACV and Ara-C also showed greater γH2AX response in the *Tdp1*$^{-/-}$ cells (Figure 5B). All these characteristics indicate that *Tdp1*$^{-/-}$ cells accumulate more DNA damage when treated with CTNAs, leading to increased cell cycle alterations and cell death. These results suggest that, in addition to repairing CPT-induced damage, TDP1 repairs 3′-blocking lesions induced by therapeutic CTNAs.

Table 2. IC_{50} values of CTNAs for wild-type and *Tdp1*$^{-/-}$ cells

CTNAs	DT40 IC_{50} (72 h)	
	Wild-type	*Tdp1*$^{-/-}$
ACV	1.25 μM	0.66 μM
Ara-C	134 nM	70 nM
Gemcitabine	1.6 μM	1.64 μM

Mitochondrial DNA depletion by AZT and ddC in *Tdp1*$^{-/-}$ cells

AZT and ddC are known to cause mitochondrial myopathy in patients undergoing long-term antiviral treatments (8,14,36). These myopathies have been attributed to the relaxed selectivity of mitochondrial DNA polγ, allowing significant incorporation of CTNAs (37,38). Because TDP1 localizes to the mitochondria (22,39), we investigated whether TDP1 could be involved in the repair of CTNA-induced mitochondrial DNA (mtDNA) damage. Wild-type and *Tdp1*$^{-/-}$ DT40 cells were treated with AZT or ddC for 24 h. Fluorescence-activated cell sorting analysis of cells stained with a mitochondria membrane specific dye, 10 N nonyl-acridine orange, showed that treatment with AZT or ddC did not change the mitochondria mass of either wild-type or *Tdp1*$^{-/-}$ cells (data not shown). The genomic DNA was extracted from treated and untreated samples and subjected to qPCR analysis. The resulting mtDNA copy numbers for all samples were normalized to those of the untreated wild-type or *Tdp1*$^{-/-}$ cells, respectively. Although treatment with 40 μM AZT had no impact on mtDNA copy number of wild-type DT40 cells, it reduced the mtDNA copy number of *Tdp1*$^{-/-}$ DT40 cells by ~50% (Figure 6). Treatment with higher concentration of AZT induced stress-induced mitochondrial biogenesis in wild-type cells, resulting in a 50% increase in mtDNA copy number (18), whereas such normal response was absent in *Tdp1*$^{-/-}$ cells (Figure 6). Treatment with ddC, a CTNA commonly used to deplete mtDNA in cells, led to greater reduction in mtDNA copy number in *Tdp1*$^{-/-}$ cells in comparison with wild-type cells (Figure 6). These findings implicate TDP1 in the repair of mtDNA damage induced by CTNAs.

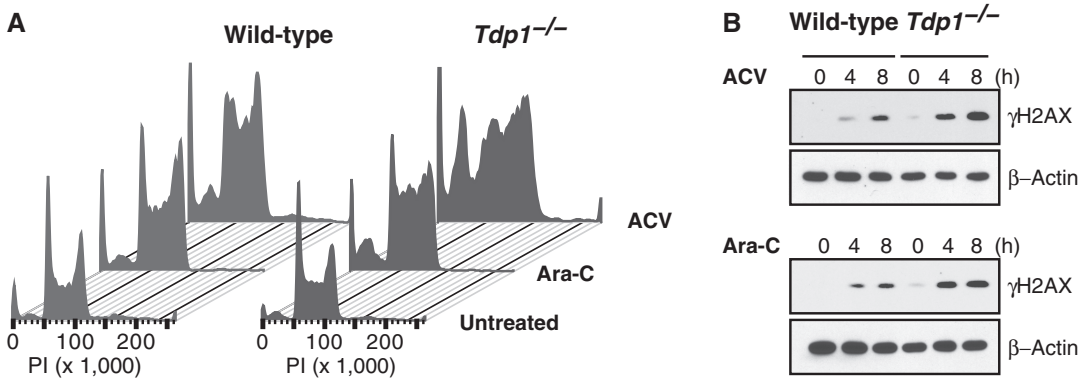

Figure 5. *Tdp1*$^{-/-}$ DT40 cells treated with CTNAs show enhanced perturbations in cell cycle profiles and greater DNA damage. (**A**) Wild-type and *Tdp1*$^{-/-}$ DT40 cells were treated with 5 μM ACV or 150 nM Ara-C for 24 h before cell cycle analysis. (**B**) Western blots of wild-type and *Tdp1*$^{-/-}$ DT40 cells treated with 2.5 μM ACV or 200 nM Ara-C probed for γH2AX are shown. β′-actin served as loading control, and the length of continuous drug treatment is indicated above each lane.

DISCUSSION

ACV, Ara-C, AZT and ddC all belong to a class of widely used CTNA drugs (3–5). They interfere with several important aspects of normal metabolisms in cells, including directly disrupting DNA replication by acting as competitive substrates for DNA polymerases. Depending on its particular biochemical properties, each CTNA attains its therapeutic selectivity through a combination of differential phosphorylation by host and viral kinases, as well as differential misincorporation by host and viral polymerases. Understanding how cells repair the DNA damage induced by CTNAs carries important implications for the medical uses of these drugs in anticancer and antiviral therapy.

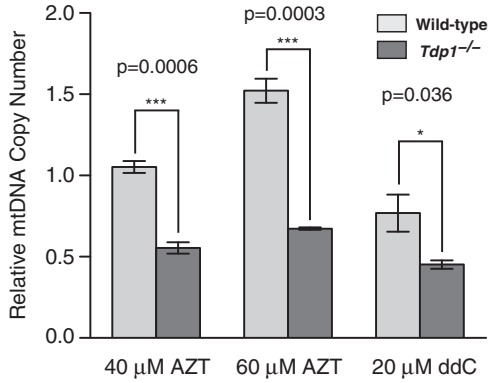

Figure 6. Depletion of mtDNA in AZT- and ddC-treated *Tdp1*$^{-/-}$ cells. The relative mitochondria DNA copy numbers of wild-type and *Tdp1*$^{-/-}$ DT40 cells were determined using quantitative real-time PCR in triplicates or quintuplets post-treatment with the indicated drug concentrations for 24 h. Mitochondrial DNA copy numbers of untreated wild-type and *Tdp1*$^{-/-}$ DT40 cells were set as 1. Relative mtDNA copy numbers of treated cells were normalized to the untreated cell in their respective cell type. At least three independent experiments were averaged, and the error bars represent SEM. A two-tailed *t*-test was carried out ($n \geq 3$), with the *P*-value for each group shown above the bars.

Here, we investigated the role of TDP1 in response to four clinically relevant CTNAs, as TDP1 is capable of removing a single nucleoside from DNA 3′-ends (40). Our results demonstrate that the 3′-nucleosidase activity of recombinant TDP1 is capable of excising 3′-CTNA *in vitro*. ACV and Ara-C led to reduced survival and greater DNA damage in *Tdp1*$^{-/-}$ DT40 and MEF cells, indicative of functional relevance for TDP1 in repairing DNA damage induced by CTNAs. The concentrations used in our study are clinically relevant, as they approximate the reported physiological plasma concentrations in patients receiving ACV (peak plasma concentration of 16–25 μM for suppression therapy for herpes simplex) (41,42) or Ara-C (plasma concentration in the micromolar range) (43,44). We also show that mtDNA depletion induced by AZT and ddC was aggravated in *Tdp1*$^{-/-}$ cells.

Our data provide evidence for a novel role of TDP1 in the removal of CTNAs (Figure 7). The broad specificity of TDP1 is consistent with its crystal structure showing few specific protein-substrate contacts between TDP1 and the Top1-derived peptide (45). Judging from our *in vivo* results, TDP1 seems to be important for removing

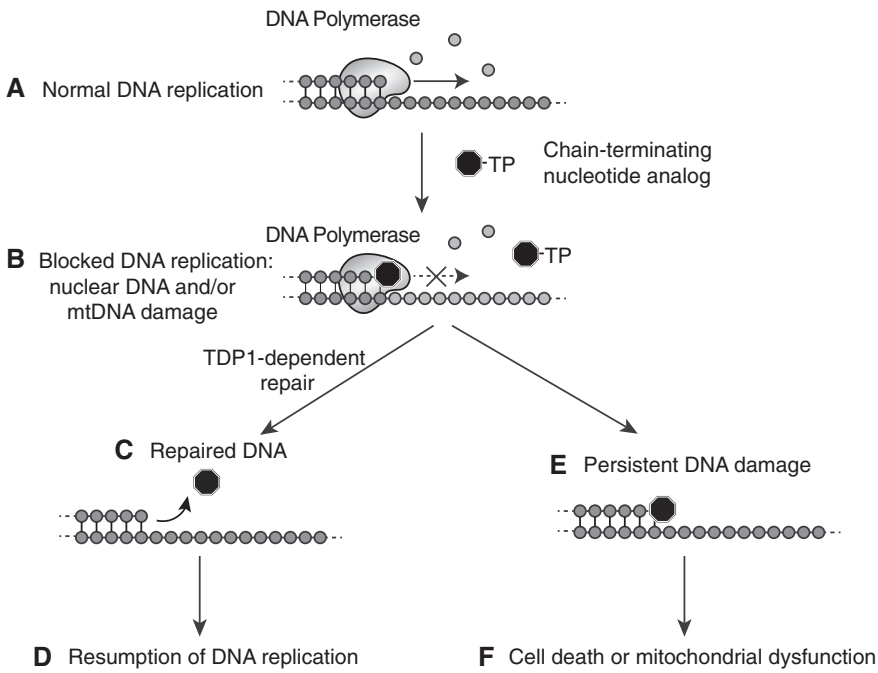

Figure 7. Proposed model for TDP1-dependent repair of nuclear or mitochondrial DNA damage induced by CTNAs. (**A**) Canonical model of DNA replication. (**B**) CTNAs (black octagon) are phosphorylated/activated to tri-phosphate form by cellular or viral kinases. The tri-phosphorylated drug acts as a competitive substrate for DNA polymerase during DNA replication and causes stalled DNA replication fork and premature termination of DNA chain. Depending on the drug, CTNA induces nuclear and/or mitochondrial DNA damage. (**C**) In the presence TDP1, TDP1-dependent repair excises the CTNA blocking the 3′-ends directly. (**D**) DNA replication is allowed to resume. (**E**) In the absence of TDP1, CTNA-induced DNA damage persists in the nuclear or mitochondrial genome. (**F**) The persistent DNA damage can lead to cell death or mitochondrial dysfunction.

CTNAs despite the apparent lower efficiency of removal *in vitro*. Because TDP1 forms repair complexes modulated by post-translational modifications (17,20,46,47), such repair complexes might survey the genome for DNA damage and further modulate local environments surrounding particular DNA damage, potentially enhancing TDP1 processing efficiencies *in vivo*.

Although Ara-C is a strong DNA chain terminator, it is also detected at internal positions in DNA chains *in vivo* (48). When the replication machinery pauses immediately after an incorporated Ara-C, a 3′-blocking lesion is generated, which is a substrate of TDP1 via its 3′-nucleosidase activity (29). When the DNA polymerase manages to continue replication past Ara-C, or when a DNA nick containing 3′-Ara-C is sealed by DNA ligases, embedded Ara-C potentially disrupts other cellular functions. Accordingly, previous reports had implicated mismatch repair and nucleotide excision repair in Ara-C-induced response (49–51). Additionally, Ara-C near Top1-binding sites induces Top1 cleavage complexes (52); thus, we cannot rule out a possible second mechanism through which TDP1 removes Top1 cleavage complexes trapped by embedded Ara-C. However, the contribution of this second repair mechanism seems to be minor, as *Tdp1*$^{-/-}$ cells did not show hypersensitivity toward gemcitabine, which induces higher levels of Top1 cleavage complexes than Ara-C (53).

Antiviral CTNAs can lead to mitochondrial toxicity, which is attributed to their incorporation by the less selective mitochondrial polγ (7,8). However, little is known about the repair of CTNA-induced mtDNA damage. Our finding that mtDNA is selectively depleted in *Tdp1*$^{-/-}$ cells treated with AZT and ddC suggests a role for TDP1 in the repair of CTNA-induced mtDNA damage.

TDP1 is regarded as a logical target for anticancer chemotherapies because TDP1 inhibitors may selectively enhance the efficacy of Top1 poisons in cancer cells (28,54,55). Elucidation of this novel TDP1-dependent repair pathway for CTNAs suggests that anticancer treatment could also benefit from the synergistic effect of Ara-C and TDP1 inhibitors in combinational therapy.

ACKNOWLEDGEMENTS

The authors thank Dr Cornelius F. Boerkoel (Center for Molecular Medicine and Therapeutics; University of British Columbia, Canada) for the kind gift of wild-type and *Tdp1*$^{-/-}$ MEF cells.

FUNDING

Intramural Program of the National Cancer Institute, Center for Cancer Research [Z01 BC006150]; NIH-NCI [U01 CA102532]. Funding for open access charge: Intramural Program of the National Cancer Institute, Center for Cancer Research [Z01 BC006150].

Conflict of interest statement. None declared.

REFERENCES

1. De Clercq,E. and Field,H.J. (2006) Antiviral prodrugs - the development of successful prodrug strategies for antiviral chemotherapy. *Br. J. Pharmacol.*, **147**, 1–11.
2. Berdis,A.J. (2008) DNA polymerases as therapeutic targets. *Biochemistry*, **47**, 8253–8260.
3. Schaeffer,H.J., Beauchamp,L., de Miranda,P., Elion,G.B., Bauer,D.J. and Collins,P. (1978) 9-(2-hydroxyethoxymethyl) guanine activity against viruses of the herpes group. *Nature*, **272**, 583–585.
4. Rashbaum,S.A. and Cozzarelli,N.R. (1976) Mechanism of DNA synthesis inhibition by arabinosyl cytosine and arabinosyl adenine. *Nature*, **264**, 679–680.
5. Mitsuya,H., Yarchoan,R. and Broder,S. (1990) Molecular targets for AIDS therapy. *Science*, **249**, 1533–1544.
6. Nickel,W., Austermann,S., Bialek,G. and Grosse,F. (1992) Interactions of azidothymidine triphosphate with the cellular DNA polymerases alpha, delta, and epsilon and with DNA primase. *J. Biol. Chem.*, **267**, 848–854.
7. Johnson,A.A., Ray,A.S., Hanes,J., Suo,Z., Colacino,J.M., Anderson,K.S. and Johnson,K.A. (2001) Toxicity of antiviral nucleoside analogs and the human mitochondrial DNA polymerase. *J. Biol. Chem.*, **276**, 40847–40857.
8. Lee,H., Hanes,J. and Johnson,K.A. (2003) Toxicity of nucleoside analogues used to treat AIDS and the selectivity of the mitochondrial DNA polymerase. *Biochemistry*, **42**, 14711–14719.
9. Iwasaki,H., Huang,P., Keating,M.J. and Plunkett,W. (1997) Differential incorporation of ara-C, gemcitabine, and fludarabine into replicating and repairing DNA in proliferating human leukemia cells. *Blood*, **90**, 270–278.
10. Richardson,K.A., Vega,T.P., Richardson,F.C., Moore,C.L., Rohloff,J.C., Tomkinson,B., Bendele,R.A. and Kuchta,R.D. (2004) Polymerization of the triphosphates of AraC, 2′,2′-difluorodeoxycytidine (dFdC) and OSI-7836 (T-araC) by human DNA polymerase alpha and DNA primase. *Biochem. Pharmacol.*, **68**, 2337–2346.
11. Prakasha Gowda,A.S., Polizzi,J.M., Eckert,K.A. and Spratt,T.E. (2010) Incorporation of gemcitabine and cytarabine into DNA by DNA polymerase beta and ligase III/XRCC1. *Biochemistry*, **49**, 4833–4840.
12. Sampath,D., Rao,V.A. and Plunkett,W. (2003) Mechanisms of apoptosis induction by nucleoside analogs. *Oncogene*, **22**, 9063–9074.
13. Lewis,W., Day,B.J. and Copeland,W.C. (2003) Mitochondrial toxicity of NRTI antiviral drugs: an integrated cellular perspective. *Nat Rev. Drug Discov.*, **2**, 812–822.
14. Hanes,J.W. and Johnson,K.A. (2007) A novel mechanism of selectivity against AZT by the human mitochondrial DNA polymerase. *Nucleic Acids Res.*, **35**, 6973–6983.
15. Pouliot,J.J., Yao,K.C., Robertson,C.A. and Nash,H.A. (1999) Yeast gene for a Tyr-DNA phosphodiesterase that repairs topoisomerase I complexes. *Science*, **286**, 552–555.
16. Hirano,R., Interthal,H., Huang,C., Nakamura,T., Deguchi,K., Choi,K., Bhattacharjee,M.B., Arimura,K., Umehara,F., Izumo,S. *et al.* (2007) Spinocerebellar ataxia with axonal neuropathy: consequence of a Tdp1 recessive neomorphic mutation? *EMBO J.*, **26**, 4732–4743.
17. Das,B.B., Antony,S., Gupta,S., Dexheimer,T.S., Redon,C.E., Garfield,S., Shiloh,Y. and Pommier,Y. (2009) Optimal function of the DNA repair enzyme TDP1 requires its phosphorylation by ATM and/or DNA-PK. *EMBO J.*, **28**, 3667–3680.
18. Fu,X., Wan,S., Lyu,Y.L., Liu,L.F. and Qi,H. (2008) Etoposide induces ATM-dependent mitochondrial biogenesis through AMPK activation. *PloS One*, **3**, e2009.
19. Miao,Z.H., Agama,K., Sordet,O., Povirk,L., Kohn,K.W. and Pommier,Y. (2006) Hereditary ataxia SCAN1 cells are defective for the repair of transcription-dependent topoisomerase I cleavage complexes. *DNA Repair*, **5**, 1489–1494.
20. El-Khamisy,S.F., Saifi,G.M., Weinfeld,M., Johansson,F., Helleday,T., Lupski,J.R. and Caldecott,K.W. (2005) Defective DNA single-strand break repair in spinocerebellar ataxia with axonal neuropathy-1. *Nature*, **434**, 108–113.

21. Zhou,T., Lee,J.W., Tatavarthi,H., Lupski,J.R., Valerie,K. and Povirk,L.F. (2005) Deficiency in 3′-phosphoglycolate processing in human cells with a hereditary mutation in tyrosyl-DNA phosphodiesterase (TDP1). *Nucleic Acids Res.*, **33**, 289–297.
22. Das,B.B., Dexheimer,T.S., Maddali,K. and Pommier,Y. (2010) Role of tyrosyl-DNA phosphodiesterase (TDP1) in mitochondria. *Proc. Natl Acad. Sci. USA*, **107**, 19790–19795.
23. Murai,J., Huang,S.N., Das,B.B., Dexheimer,T.S., Takeda,S. and Pommier,Y. (2012) Tyrosyl-DNA phosphodiesterase 1 (TDP1) repairs DNA damage induced by topoisomerases I and II and base alkylation in vertebrate cells. *J. Biol. Chem.*, **287**, 12848–12857.
24. Takashima,H., Boerkoel,C.F., John,J., Saifi,G.M., Salih,M.A.M., Armstrong,D., Mao,Y., Quiocho,F.A., Roa,B.B., Nakagawa,M. *et al.* (2002) Mutation of TDP1, encoding a topoisomerase I-dependent DNA damage repair enzyme, in spinocerebellar ataxia with axonal neuropathy. *Nat. Genet.*, **32**, 267–272.
25. Katyal,S., el-Khamisy,S.F., Russell,H.R., Li,Y., Ju,L., Caldecott,K.W. and McKinnon,P.J. (2007) TDP1 facilitates chromosomal single-strand break repair in neurons and is neuroprotective *in vivo*. *EMBO J.*, **26**, 4720–4731.
26. Dexheimer,T.S., Stephen,A.G., Fivash,M.J., Fisher,R.J. and Pommier,Y. (2010) The DNA binding and 3′-end preferential activity of human tyrosyl-DNA phosphodiesterase. *Nucleic Acids Res.*, **38**, 2444–2452.
27. Antony,S., Marchand,C., Stephen,A.G., Thibaut,L., Agama,K.K., Fisher,R.J. and Pommier,Y. (2007) Novel high-throughput electrochemiluminescent assay for identification of human tyrosyl-DNA phosphodiesterase (Tdp1) inhibitors and characterization of furamidine (NSC 305831) as an inhibitor of Tdp1. *Nucleic Acids Res.*, **35**, 4474–4484.
28. Dexheimer,T.S., Antony,S., Marchand,C. and Pommier,Y. (2008) Tyrosyl-DNA phosphodiesterase as a target for anticancer therapy. *Anticancer Agents Med. Chem.*, **8**, 381–389.
29. Interthal,H., Chen,H.J. and Champoux,J.J. (2005) Human Tdp1 cleaves a broad spectrum of substrates, including phosphoamide linkages. *J. Biol. Chem.*, **280**, 36518–36528.
30. Yang,S.W., Burgin,A.B., Huizenga,B.N., Robertson,C.A., Yao,K.C. and Nash,H.A. (1996) A eukaryotic enzyme that can disjoin dead-end covalent complexes between DNA and type I topoisomerases. *Proc. Natl Acad. Sci. USA*, **93**, 11534–11539.
31. Raymond,A.C., Staker,B.L. and Burgin,A.B. (2005) Substrate specificity of tyrosyl-DNA phosphodiesterase I (Tdp1). *J. Biol. Chem.*, **280**, 22029–22035.
32. Raymond,A.C., Rideout,M.C., Staker,B., Hjerrild,K. and Burgin,A.B. (2004) Analysis of human tyrosyl-DNA phosphodiesterase I catalytic residues. *J. Mol. Biol.*, **338**, 895–906.
33. Kim,H., Na,S.H., Lee,S.Y., Jeong,Y.M., Hwang,H.J., Hur,J.Y., Park,S.H., Woo,J.C. and Kim,S.G. (2012) Structure-function studies of a plant tyrosyl-DNA phosphodiesterase provide novel insights into DNA repair mechanisms of Arabidopsis thaliana. *Biochemical. J.*, **443**, 49–56.
34. Gottlin,E.B., Rudolph,A.E., Zhao,Y., Matthews,H.R. and Dixon,J.E. (1998) Catalytic mechanism of the phospholipase D superfamily proceeds via a covalent phosphohistidine intermediate. *Proc. Natl Acad. Sci. USA*, **95**, 9202–9207.
35. Huang,P., Chubb,S., Hertel,L.W., Grindey,G.B. and Plunkett,W. (1991) Action of 2′,2′-difluorodeoxycytidine on DNA synthesis. *Cancer Res.*, **51**, 6110–6117.
36. Chen,C.H. and Cheng,Y.C. (1989) Delayed cytotoxicity and selective loss of mitochondrial DNA in cells treated with the anti-human immunodeficiency virus compound 2′,3′-dideoxycytidine. *J. Biol. Chem.*, **264**, 11934–11937.
37. Lim,S.E. and Copeland,W.C. (2001) Differential incorporation and removal of antiviral deoxynucleotides by human DNA polymerase gamma. *J. Biol. Chem.*, **276**, 23616–23623.
38. Feng,J.Y., Johnson,A.A., Johnson,K.A. and Anderson,K.S. (2001) Insights into the molecular mechanism of mitochondrial toxicity by AIDS drugs. *J. Biol. Chem.*, **276**, 23832–23837.
39. Fam,H.K., Chowdhury,M.K., Walton,C., Choi,K., Boerkoel,C.F. and Hendson,G. (2013) Expression profile and mitochondrial colocalization of Tdp1 in peripheral human tissues. *J. Mol. Histol.*, **44**, 481–494.
40. Interthal,H., Chen,H.J., Kehl-Fie,T.E., Zotzmann,J., Leppard,J.B. and Champoux,J.J. (2005) SCAN1 mutant Tdp1 accumulates the enzyme–DNA intermediate and causes camptothecin hypersensitivity. *EMBO J.*, **24**, 2224–2233.
41. Beutner,K.R., Friedman,D.J., Forszpaniak,C., Andersen,P.L. and Wood,M.J. (1995) Valaciclovir compared with acyclovir for improved therapy for herpes zoster in immunocompetent adults. *Antimicrob. Agents Chemother.*, **39**, 1546–1553.
42. Soul-Lawton,J., Seaber,E., On,N., Wootton,R., Rolan,P. and Posner,J. (1995) Absolute bioavailability and metabolic disposition of valaciclovir, the L-valyl ester of acyclovir, following oral administration to humans. *Antimicrob. Agents Chemother.*, **39**, 2759–2764.
43. Powis,G. (1983) Dose-dependent metabolism, therapeutic effect, and toxicity of anticancer drugs in man. *Drug Metab. Rev.*, **14**, 1145–1163.
44. Capizzi,R.L., White,J.C., Powell,B.L. and Perrino,F. (1991) Effect of dose on the pharmacokinetic and pharmacodynamic effects of cytarabine. *Sem. Hematol.*, **28**, 54–69.
45. Davies,D.R., Interthal,H., Champoux,J.J. and Hol,W.G. (2003) Crystal structure of a transition state mimic for Tdp1 assembled from vanadate, DNA, and a topoisomerase I-derived peptide. *Chem. Biol.*, **10**, 139–147.
46. Plo,I., Liao,Z.Y., Barcelo,J.M., Kohlhagen,G., Caldecott,K.W., Weinfeld,M. and Pommier,Y. (2003) Association of XRCC1 and tyrosyl DNA phosphodiesterase (Tdp1) for the repair of topoisomerase I-mediated DNA lesions. *DNA Repair*, **2**, 1087–1100.
47. Hudson,J.J., Chiang,S.C., Wells,O.S., Rookyard,C. and El-Khamisy,S.F. (2012) SUMO modification of the neuroprotective protein TDP1 facilitates chromosomal single-strand break repair. *Nat. Commun.*, **3**, 733.
48. Major,P.P., Egan,E.M., Beardsley,G.P., Minden,M.D. and Kufe,D.W. (1981) Lethality of human myeloblasts correlates with the incorporation of arabinofuranosylcytosine into DNA. *Proc. Natl Acad. Sci. USA*, **78**, 3235–3239.
49. Takahashi,T., Min,Z., Uchida,I., Arita,M., Watanabe,Y., Koi,M. and Hemmi,H. (2005) Hypersensitivity in DNA mismatch repair-deficient colon carcinoma cells to DNA polymerase reaction inhibitors. *Cancer Lett.*, **220**, 85–93.
50. Fordham,S.E., Matheson,E.C., Scott,K., Irving,J.A.E. and Allan,J.M. (2011) DNA mismatch repair status affects cellular response to Ara-C and other anti-leukemic nucleoside analogs. *Leukemia*, **25**, 1046–1049.
51. Wu,Q., Beland,F.A., Chang,C.W. and Fang,J.L. (2011) XPC is essential for nucleotide excision repair of zidovudine-induced DNA damage in human hepatoma cells. *Toxicol. Appl. Pharmacol.*, **251**, 155–162.
52. Pourquier,P., Takebayashi,Y., Urasaki,Y., Gioffre,C., Kohlhagen,G. and Pommier,Y. (2000) Induction of topoisomerase I cleavage complexes by 1-beta -D-arabinofuranosylcytosine (ara-C) *in vitro* and in ara-C-treated cells. *Proc. Natl Acad. Sci. USA*, **97**, 1885–1890.
53. Pourquier,P., Gioffre,C., Kohlhagen,G., Urasaki,Y., Goldwasser,F., Hertel,L.W., Yu,S., Pon,R.T., Gmeiner,W.H. and Pommier,Y. (2002) Gemcitabine (2′,2′-difluoro-2′-deoxycytidine), an antimetabolite that poisons topoisomerase I. *Clin. Cancer Res.*, **8**, 2499–2504.
54. Huang,S.N., Pommier,Y. and Marchand,C. (2011) Tyrosyl-DNA Phosphodiesterase 1 (Tdp1) inhibitors. *Expert Opin. Ther. Pat.*, **21**, 1285–1292.
55. Zhang,Y.W., Regairaz,M., Seiler,J.A., Agama,K.K., Doroshow,J.H. and Pommier,Y. (2011) Poly(ADP-ribose) polymerase and XPF-ERCC1 participate in distinct pathways for the repair of topoisomerase I-induced DNA damage in mammalian cells. *Nucleic Acids Res.*, **39**, 3607–3620.